RSC Advances

ROYAL SOCIETY
OF CHEMISTRY

www.rsc.org/advances

Investigation of the tunable properties of

graphene complementary terahertz metamaterials

Xiaoyong He[1,*], Chunlin Liu[1], Xu Zhong[2], and Wangzhou Shi[1]

[1]Department of Physics, Mathematics & Science College,

Shanghai Normal University, No. 100 Guilin Road, Shanghai, 200234, P. R. China

[2]School of Electronics and Information, Shanghai Dianji University, 690 Jiangchuan Road,

Shanghai, 200240, P. R. of China

Abstract: Based on the graphene-SiO_2-Si structure, the tunable resonant properties of the complementary graphene metamaterials (MMs) have been investigated in the terahertz regime. The influence of operation frequency, the Fermi levels of graphene layer, and different kinds of graphene patterns have been taken into account. The results manifest that the tunable mechanisms of the complementary graphene MMs structures mainly depend on the *LC* resonance. The resonant transmission and reflection properties of the complementary graphene MMs structures can be tuned in a wide range via controlling the applied electric fields. As the Fermi level of graphene layer increases, the resonances of the MMs structure become stronger, and the resonant peaks of the transmission curves shift to the higher frequency, resulting from the permittivity of graphene layer increases in the THz regime. The transmission (reflection) spectrum is broad (sharp), which can be used to fabricate transmission modulator (reflection filters). The results are very helpful to design novel plasmonic devices

and useful for the application of biomedical sensing and optical communications.

1. Introduction

Recently, terahertz (THz) science and technology have made rapid development [1-7], but compared to the well-established neighboring infrared and microwave wavebands, THz regime is still in need of fundamental advancement. One big challenge to develop THz technology further is that it is very difficult to find suitable materials to respond the THz radiation strongly. Fortunately, this problem can be alleviate to a large extend with the help of metamaterials (MMs) [8, 9], which provides a promising platform for the investigation of many phenomena, such as negative refractive index [10], super focusing [11], and extraordinary transmission [12, 13]. Additionally, according to the Babinet equivalent rule, the complementary MMs (c-MMs) can also offer a simple means to control over the electromagnetic wave propagation [14] and have been proven to effectively manage the propagation wave within the guided wave structure [15]. Being for the most part opaque, the c-MMs are very suited to act as reflectors, antenna or confining controlled impedance surfaces [16, 17]. But the above-mentioned MMs structures with the determined geometrical parameters can operate only at a fixed frequency, limiting actual applicability. For the actively controlled MMs, whose responses can be tuned by the application of an external stimulus even after fabrication, the variety applications can be extended tremendously [18]. Some tunable active MMs devices based were shown [19]. For instance, by incorporating semiconductors in the critical regions MMs SRRs, the frequency agile devices can operate as a broadband THz modulators due to the causal relation between the amplitude modulation and phase shifting [20].

With the merits of high carrier mobility and strong interaction with light in a broad frequency regimes [21-25], graphene, has attracted considerable

attention for both fundamental physics and enormous applications [26-28], which can be regarded as an alternative to traditional metallic materials and serve as a good platform for surface plasmons (SPs) [29-31]. The linear dispersion of the 2D Dirac fermions also provides ultra-wide band tunability through electrostatic field, magnetic field or chemical doping [13, 32-35]. By structuring graphene membrane and forming well-defined resonances, tunable active MMs can be also obtained. Nowadays, there are some theoretical and experimental investigations in this aspect. Ding *et al* numerically investigated the single and multiple transparency windows in the Mid-IR spectral region on the base of graphene monolayer perforated with quad-rupole and dolmen-like slot structure, which displayed that the transparency windows was controlled over a broad frequency range by varying the Fermi energy levels [36]. With the integrated graphene layer, the substantial gate-induced persistent switch and linear modulation of THz waves was shown, which also indicated the persistent photonic memory effects [37]. By depositing the metal sub-wavelength ring apertures on the graphene-SiO_2-Si layers, Gao *et al.* suggested the high speed modulators, manifesting that the amplitude modulation of THz waves can reach about 50% [38].

As the key waveguides devices, the modulators and reflectors are highly required to meet the needs of the THz wireless communication or ultrafast inter-connects [39]. Regretfully, there still exist many problems for current state-of-the-art devices, such as the small modulation depth, low modulation speed and the requirement of cryogenic temperatures. Therefore, further improvement of the device performance characteristics is needed for the practical applications. By depositing the graphene patterns on the flexible substrate, we propose the complementary graphene-SiO_2-Si (c-$GSiO_2Si$) structures to realize dynamic control of the propagation waves. The tunable propagation properties of the proposed c-$GSiO_2G$ structure have been

theoretically explored in the THz regime, including the effects of operation frequency, Fermi level and different kinds of graphene patterns.
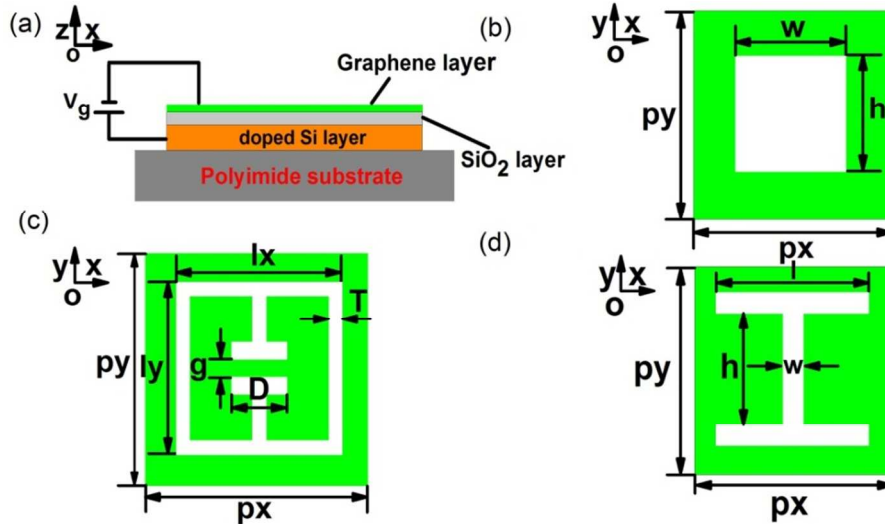
2. THEORETIC MODEL AND RESEARCH METHOD

Figure1 The side view of the graphene complementary MMs structure, the graphene patterns are deposited on the SiO$_2$/Si layers, the thickness of the SiO$_2$ layer is 30 *nm*, the doped Si layer with the thickness of 1 μm is used to apply the gate voltage. The substrate is made from the polyimide layer. Fig. 1(b)-1(d) The top views of geometry and dimensions of the several kinds of MMs unit cell structures. Fig. 1(b) the rectangle structure, *w=h=*36 μm; Fig.1(c) the eSRRs structure, $l_x=l_y=$ 36μm, *g*= 2 μm, *D*= 10 μm, *T*= 4 μm; Fig. 1(d) the H-shaped structure, *w=*6μm, *h=*36 μm, and *l=*48 μm; The periodic length along *x* and *y* directions are both 60 μm. The green shaded regions indicate the graphene layer, and the gray layer is the SiO$_2$.

Figure 1(a) shows the sketch of the top view of the complementary graphene MMs structure, which print on the SiO$_2$/doped-Si wafer. The thicknesses of the SiO$_2$ and Si layers are 30 *nm* and 1 *μm*, respectively. To reduce the influence of the substrate, the flexible dielectric layer is adopted, which is made from the polyimide layer with the thickness of 2 *μm*. Figure 1(b)-1(d) show the top views of the geometry for several kinds of MMs unit cell structures, the rectangular (Fig. 1b), the eSRRs-shaped (Fig. 1c), and the H-shaped unit cell structures (Fig. 1d). The period lengths along *x* and *y* directions are d_x and d_y, respectively. The complementary MMs structures are made of monolayer graphene with the thickness of 0.34 *nm*. The incident

waves normally transmit through the c-GSiO$_2$Si structure along z direction.

Graphene can be considered as a 2D material and described by a surface conductivity σ_g, which is related to the radiation frequency ω, chemical potential (μ_c, Fermi level E_f), the environmental temperature T, and the relaxation time τ. The conductivity of the monolayer graphene can be calculated by using the Kubo formula [40]:

$$\sigma(\omega,\mu_c,\tau,T)=\sigma_{inter}+\sigma_{intra}=\frac{je^2\left(\omega-j\tau^{-1}\right)}{\pi\hbar^2}\times$$

$$\left[\frac{1}{\left(\omega-j\tau^{-1}\right)^2}\int_0^\infty\frac{\partial f_d(\varepsilon)}{\partial\varepsilon}-\frac{\partial f_d(-\varepsilon)}{\partial\varepsilon}d\varepsilon-\int_0^\infty\frac{f_d(-\varepsilon)-f_d(\varepsilon)}{\left(\omega-j\tau^{-1}\right)^2-4\left(\varepsilon/\hbar\right)^2}d\varepsilon\right]$$

(1)

where $f_d(\varepsilon)$ is the Fermi-Dirac distribution, j is the imaginary unit, ε is the energy of the incident wave, k_B is Boltzmann's constant, and $\hbar$ is the reduced Planck's constant. The first part of the above equation is the intra-band contribution, and the second part contributed to the inter-band contribution.

Correspondingly, the dielectric constant of graphene layer can be expressed as:

$$\varepsilon_g=1+j\frac{\sigma_g}{\omega\varepsilon_0\Delta} \tag{2}$$

where Δ is the graphene layer thickness, ε_0 is the permittivity of free space. If the surface conductivity of the graphene layer is regarded as the isotropic frequency profile, the Fermi level can be determined by the carrier concentration:

$$n_d=\frac{1}{\pi\hbar^2v_F^2}\int f_d(\varepsilon)-f_d\left(\varepsilon+2E_f\right)\varepsilon d\varepsilon \tag{3}$$

where $v_F\approx1\times10^6$ m/s is the Fermi velocity.

3. Results and Discussions

The simulation result obtained from the well-established CST Microwave Studio, which is a 3D full-wave solver and based on the finite integration technique. The frequency domain solver adopts with the unit-cell boundary conditions in the x-y plane and Floquet ports in the *z* direction to terminate. By using the S-parameters from the simulation, the transmission ($T(\omega)$), reflection ($R(\omega)$) and absorption ($A(\omega)$) can be obtained, *i.e.* $T(\omega)=|S_{21}|^2$, $R(\omega)=|S_{11}|^2$, $A(\omega)=1.0-T(\omega)-R(\omega)$.
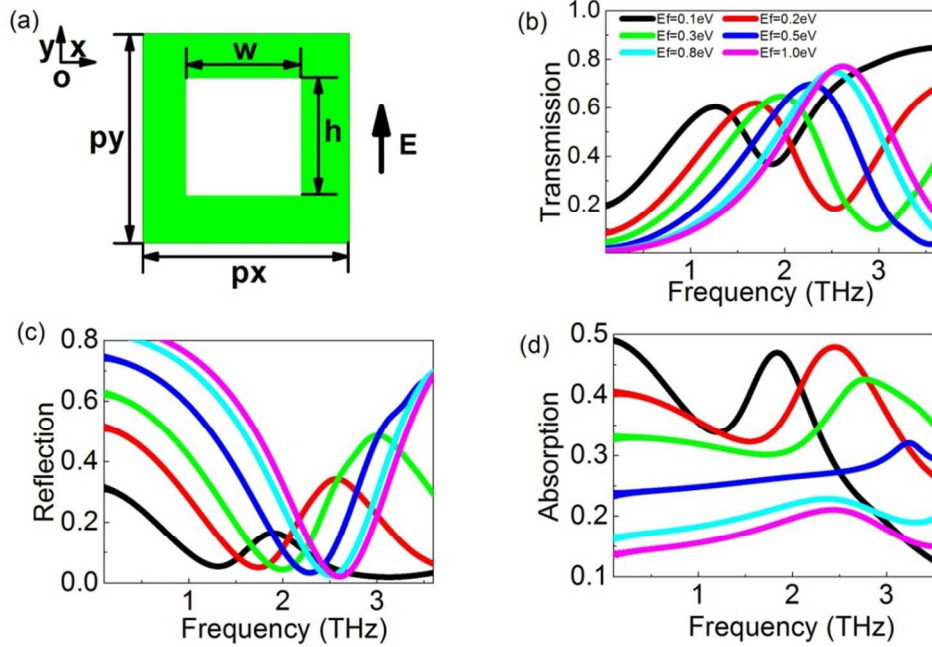

Figure 2(a) The sketch of the rectangular unit cell. The polarization of the incident wave is along *y* direction. Fig. 2(b), 2(c) and 2(d) show the transmission, reflection, and absorption curves of the graphene complementary MMs based on the rectangular shaped unit cell structure. The Fermi levels of the graphene layer are 0.1 eV, 0.2 eV, 0.3 eV, 0.5 eV, 0.8 eV, and 1.0 eV, respectively.

Figure 2 shows the propagation properties of the incident light through the c-GSiO$_2$Si structure based on the rectangular unit cell at different Fermi levels. The length and width of the cross structure are both 36 μm. The sketch of the graphene rectangular unit cell is shown in Fig. 2(a). The polarization of the incident light is along *y* direction. Each piece of the MMs is a square lattice, its periodic lengths along *x* and *y* direction (d_x and d_y) are both 60 μm.

Different from the original graphene MMs structures showing the resonant dips, the transmission of the complementary graphene rectangular-shaped structure displays the obvious resonant peaks. The possible reasons are as follows. For the original MMs structure, the normally incident THz electric field induces an array of electric dipoles at the split gaps. The electric dipoles reradiate and destructively interfere with the incident radiation, resulting into the transmission minimum. While for the complementary graphene MMs, most of THz wave is blocked by the large graphene coverage at off-resonant condition. At resonant condition, the induced electric dipole array reradiates and leads into the THz transmission maximum. Due to the symmetric structure of the rectangular-shaped, the transmission along x direction show similar properties. Thus, the rectangular-shaped structures can be used to fabricate the polarization insensitive devices. As the Fermi level of the graphene layer increases, the values of the transmission resonant peak increases and the peak position shifts to the higher frequency, *i.e.* blue shift. Compared with the conventional metallic structure, the transmission of the proposed c-$GSiO_2Si$ structure can be tuned in a wide range by adjusting the Fermi level of the graphene layer. As the Fermi level of the graphene layer increases, the transmission of the c-$GSiO_2Si$ structure increases significantly. When the Fermi level of the graphene layer changes in the range of 0.1-1.0 eV, the resonant frequency of the transmission can be modulated in the range of 1.25-2.62 THz, and the value of the transmission can be tuned in the range of 0.60-0.77. Accordingly, the modulation depth of the frequency (f_{mod}, $f_{mod}=\Delta f/f_{max}$) is 52.3%, and the modulation depth of the transmission (T_{mod}, $T_{mod}=\Delta T/T_{max}$) is 22.1%. This can be explained by the fact that the graphene's effective permittivity increases with the Fermi level in the THz regime. As the increase of the graphene Fermi level, the dielectric constant of graphene increases, resulting into the resonant transmission become stronger. For instance, at the frequency of 1 *THz*, when the Fermi level of the graphene layer are 0.1 *eV*, 0.2

eV, and 0.5 *eV*, the permittivity of the graphene layer are $-3.60\times10^5+2.22\times10^5 i$, $-7.14\times10^5+4.40\times10^5 i$, and $-1.78\times10^6+1.10\times10^6 i$, respectively. Figure 2(c) and 2(d) show the reflection and absorption curves vs. frequency, respectively. As the Fermi level of the graphene layer increases, the reflection increases and the absorption decreases. When the Fermi level changes in the range of 0.1-1.0 eV, the resonant frequency of the reflection curve can be tuned in the range of 1.31-2.60 THz, and the value of the reflection can be modulated in the range of 0.02-0.06. The modulation depth of the frequency is 49.6%, and the modulation depth of the reflection (R_{mod}, $R_{mod}=\Delta R/R_{max}$) is 66.7%. It should also be noted that when the Fermi level of the graphene layer is low, the absorption dominates. Though the influences of the graphene layer Fermi level on the resonant frequency is significant, but its effect on the reflection amplitude is not obvious. The last but not least, the resonant transmission spectrum of the c-GSiO$_2$Si structure is relatively broad, the suggested graphene supported MMs structure are very suitable for fabricating the broadband modulators instead of the filters or switchers.
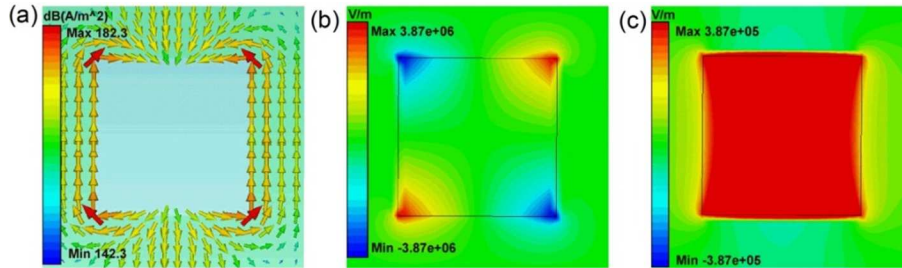

Figure 3(a)-3(c) show the surface current density, E_x and E_y of the graphene MMs structures based on the rectangular-shaped unit cell. The polarization direction of the incident light is along *y* direction. The resonant frequency is 2.62 THz. The Fermi level of the graphene layer is 1.0 eV.

Figure 3(a)-3(c) nicely illustrates the nature of the current and *x* (E_x) and *y* (E_y) components of the electric field for the graphene complementary MMs structures based on the rectangular-shaped unit cell. The polarized direction is along *y* direction. The Fermi level of the graphene layer is 1.0 *eV*. The simulation result plots at the resonant frequency of 2.62 *THz*, which

corresponds with the resonant peaks shown in Fig. 2(b). The direction and size of the arrows in Fig. 3(a) indicate the direction and relative value of the surface current density, and the color map in Fig. 3(b) and 3(c) show the relative local electric field amplitude. It can be found from Fig. 3 that for the graphene complementary MMs structures, the graphene patterns regions shows high surface current density, while the empty section corresponds to the large local electric fields, which is inversely different from the original graphene MMs structures.
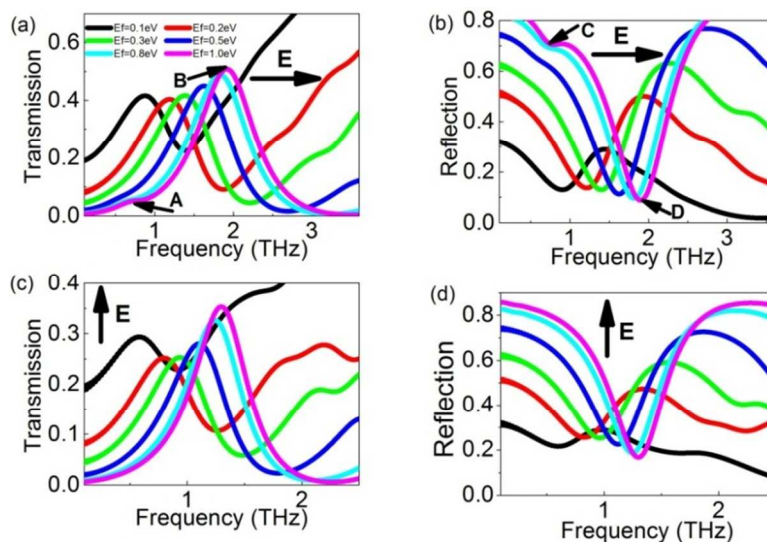

Figure 4(a) and 4(b) show the transmission and reflection of the complementary graphene MMs based on the eSRRs unit cell, the polarization of the incident wave is along x direction. Fig. 4(c) and 4(d) show the transmission and reflection of the complementary graphene MMs based on the eSRRs unit cell, the polarization of the incident wave is along y direction. The Fermi levels of the graphene layer are 0.1 eV, 0.2 eV, 0.3 eV, 0.5 eV, 0.8 eV, and 1.0 eV, respectively.

In order to compare the results with the conventionally metal complementary MMs structure, we investigate the transmission of the graphene based eSRRs structure. The geometric structure parameter of the eSRRs unit cell is shown in the caption of Fig. 1(c). Figure 4(a) and 4(b) show that the transmission and reflection curves, the polarization direction is along x direction. Besides the broad resonant peaks at higher frequency (*i.e.* peak "B"), there is also a small resonant peak at low frequency (*i.e.* peak "A") when the

Fermi level of the graphene layer is large, *e.g.* the resonant transmission peak at 0.78 THz when the E_f of the graphene layer is 1.0 eV. It will disappear if the Fermi level of the graphene layer is small. The resonant peak of transmission at low frequency attributes to the dipolar resonance. The graphene layer thickness is very small, so only on condition that the Fermi level is very high, the graphene layer manifests very good "metallic" properties, the dipolar resonant will happen. The surface current density and electric fields shown in Fig. 5(a)-5(c) confirms this. Because the dipolar resonance at low frequency is not significant, the modulation of the graphene MMs structures mainly depends on the *LC* resonance at high frequency. As the Fermi level of graphene layer increases, the resonant transmission of the MMs structure become stronger, and the resonant dip shifts to higher frequency. When the Fermi level of the graphene layer changes in the range of 0.1-1.0 *eV*, the resonant peaks of the transmission can be tuned in the range of 0.88-1.92 *THz*, and the values of the transmission can be modulated in the range of 0.42-0.51. Correspondingly, the modulation depth of the frequency is 54.2%, and the modulation depth of the transmission is 17.7%. In addition, Figure 4(b) shows the reflection response curves. When the Fermi level of the graphene layer is large, the reflection spectral curves show two dips, i.e. the low frequency dip (*i.e.* dip "C") and high frequency dip (*i.e.* dip "D"), which is accordance with the transmission peaks in Fig. 4(a). When the Fermi level of the graphene layer changes in the range of 0.1-1.0 *eV*, the resonant dips of the reflection curves can be tuned in the range of 0.90-1.90 *THz*, and the values of the reflection can be modulated in the range of 0.09-0.13. Correspondingly, the modulation depth of the frequency is 52.6%, and the modulation depth of the reflection is 30.8%. The results for the case that the polarization direction of the incident light is along *y* direction can be found in Fig. 4(c) and Fig. 4(d), manifesting significant *LC* resonance only. When the Fermi level of the graphene layer changes in the range of 0.1-1.0 *eV*, the

resonant dip of the transmission modulates in the range of 0.57-1.30 *THz*, and the value of the transmission of the eSRRs resonator structure is tuned in the range of 0.29-0.35, respectively. Accordingly, the modulation depth of the frequency is 56.2%, and the modulation depth of transmission is 17.1%. For the case of reflection, as shown in Fig. 4(d), when the Fermi level of the graphene layer changes in the range of 0.1-1.0 eV, the resonant dips of the reflection can be tuned in the range of 0.62-1.30 THz, and the values of the reflection can be modulated in the range of 0.17-0.22. The modulation depth of the frequency and reflection are 52.3% and 22.7%, respectively.
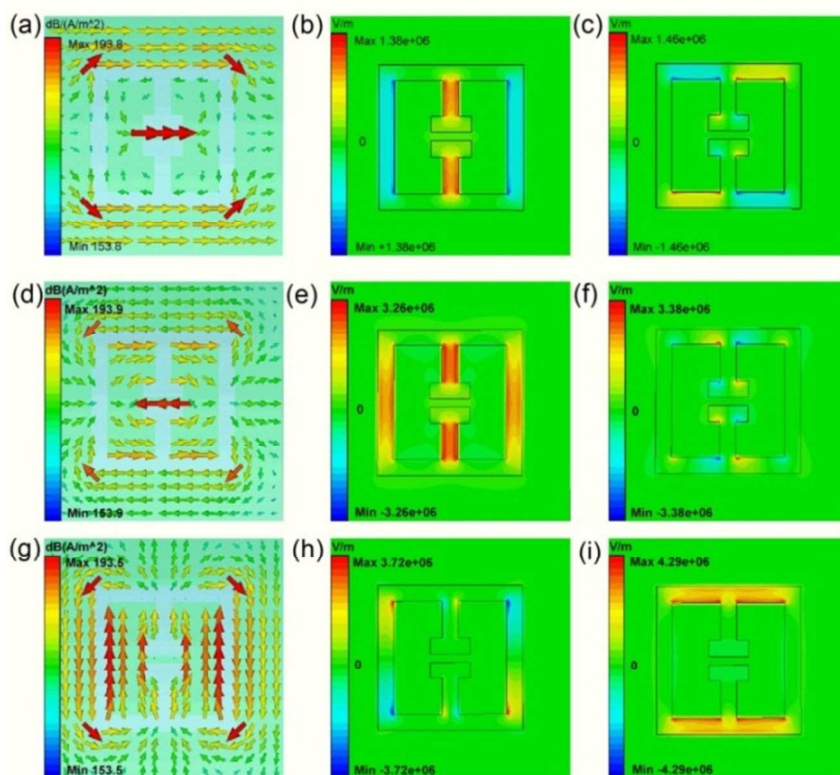

Figure 5(a)-5(c) (5(d)-5(f)) show the surface current density, E_x and E_y of the graphene complementary MMs based on the eSRRs unit cell structure at the resonant frequencies of 0.78 THz (1.92 THz). The direction of the incident light is along x direction. Fig. 5(g)-5(i) show the results when the polarization direction of the incident light along y direction. The resonant frequency is 1.30 THz. The Fermi level of the graphene layer is 1.0 eV.

Figure 5(a)-5(c) show the surface current density, the E_x and E_y components of the electric field for the *x*-polarized based on the eSRRs-

shaped MMs structure. The Fermi level of the graphene layer is 1.0 *eV*. The simulation results plot at the resonant frequency of 0.78 *THz*, which corresponds with the small resonant peak shown in Fig. 4(a). The direction and size of the arrows in Fig. 5(a) indicate the direction and relative value of the surface current density, and the color map in Fig. 5(b) and 5(c) show the relative local electric field amplitude. The simulation results in Fig. 5(a)-5(c) manifest that the resonant at low frequency is dipolar resonance. Figure 5(d)-5(f) show the surface current density, and the electric field for the *x*-polarized based on the eSRRs-shaped MMs structure at high frequency. The simulation results plots at the resonant frequency of 1.92 *THz*. The direction and size of the arrows in Fig. 5(d) indicate the direction and relative value of the surface current density, and the color map in Fig. 5(e) and 5(f) show the relative local electric field amplitude, which shows that the resonance at high frequency of 1.92 THz is *LC* resonance. The surface current density, the E_x and E_y components of the electric field for the *y*-polarized based on the complementary eSRRs-shaped MMs structure can be found in Fig. 5(g)-5(i). The resonant frequency is 1.30 *THz*, which corresponds with the resonant peak shown in Fig. 4(c). The direction and size of the arrows in Fig. 5(g) indicate the direction and relative value of the surface current density, and the color map in Fig. 5(h) and 5(i) show the relative local electric field amplitude. It can be found from Fig. 5(g)-5(i) that when the polarization is along *y* direction, the dipolar resonance disappears and only *LC* resonance exists.

Figure 6(a) and 6(b) show that the transmission and reflection response curves of the graphene MMs based on the H-shaped unit cell structures, the polarization direction is along *x* direction. When the Fermi level of the graphene layer changes in the range of 0.1-1.0 *eV*, the resonant peaks of the transmission can be tuned in the range of 0.43-0.75 *THz*, and the values of the transmission can be modulated in the range of 0.27-0.32. The values of f_{mod} and T_{mod} are 42.7% and 15.6%, respectively. The results for the reflection

curves can be found in Fig. 6(b). When the Fermi level of the graphene layer changes in the range of 0.1-1.0 *eV*, the resonant peaks of the reflection can be modulated in the range of 0.38-0.72 *THz*, and the values of the reflection can be modulated in the range of 0.19-0.24. Accordingly, the value of f_{mod} and R_{mod} are 47.2% and 20.8%, respectively. The results for the case that the polarization direction of the incident light is along *y* direction can be found in Fig. 6(c) and Fig. 6(d), respectively. As the increase of the Fermi level of the graphene layer, the amplitude of the transmission increases strongly, and the resonant peak significantly shifts to high frequency. When the Fermi level changes in the range of 0.1-1.0 *eV*, the resonant peak of the transmission modulates in the range of 0.68-1.59 *THz*, and the value of the transmission is tuned in the range of 0.44-0.56, respectively. The values of f_{mod} and T_{mod} are 57.2% and 21.4%, respectively. Additionally, in Fig. 6(d), when the Fermi level of the graphene layer changes in the range of 0.1-1.0 *eV*, the resonant dips of the reflection can be tuned in the range of 0.69-1.56 THz, and the values of the reflection can be modulated in the range of 0.069-0.11.

Figure 6(a) and 6(b) show the transmission and reflection of the complementary graphene MMs based on the H-shaped unit cell, the polarization of the incident wave is along x direction.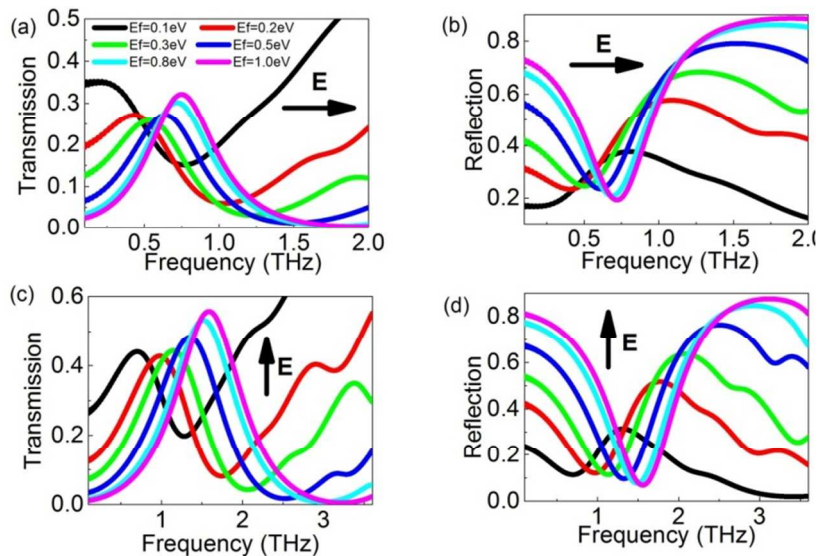 Fig. 6(c) and 6(d) show the transmission and reflection of the complementary graphene MMs based on the H-shaped unit cell, the polarization of the incident wave is along y direction.
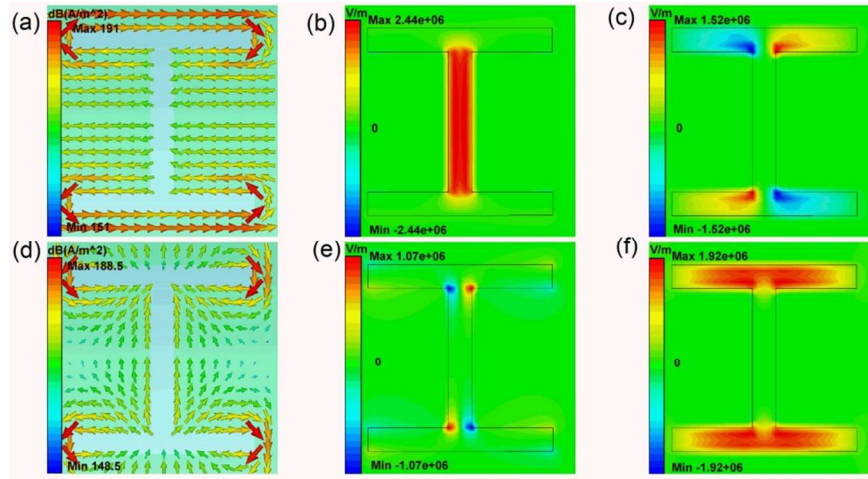
Figure 7(a)-7(c) show the surface current density, E_x and E_y of the complementary graphene MMs based on the H-shaped unit cell structure when the polarization direction of the incident light along x direction. The resonant frequency is 0.75 THz. Fig. 7(d)-7(f) show the results of the graphene MMs when the polarization direction of the incident light along y direction. The resonant frequency is 1.59 THz. The Fermi level of the graphene layer is 1.0 eV.

Figure 7(a)-7(c) show the surface current density, the E_x and E_y components of the electric field for the *x*-polarized based on the H-shaped MMs structure. The Fermi level of the graphene layer is 1.0 *eV*. The simulation results are plot at the resonant frequency of 0.75 *THz*, which is accordance with the resonant peak shown in Fig. 6(a). The direction and size of the arrows in Fig. 7(a) indicate the direction and relative value of the surface current density, and the color map in Fig. 7(b) and 7(c) show the relative local electric field amplitude. Figure 7(d)-7(f) show the surface current density, the E_x and E_y components of the electric field for the *y*-polarized. The Fermi level of the graphene layer is 1.0 eV. The simulation results are plot at the resonant frequency with the value of 1.59 THz, which is according with the resonant peak shown in Fig. 6(c). The direction and size of the arrows in Fig. 7(d) indicate the direction and relative value of the surface

current density, and the color map in Fig. 7(e) and 7(f) show the relative local electric field amplitude.

**Table 1 The comparison of
transmission properties of several kinds of different unit cell structure**

Unit cell structure	Polarized direction	f_{min}-f_{max} (THz)	Δf /f_{max} (%)	T_{min}-T_{max}	ΔT/T_{max} (%)
rectangular	x	1.25-2.62	52.29	0.60-0.77	22.08
	y	1.25-2.62	52.29	0.60-0.77	22.08
c-eSRRs	x	0.88-1.92	54.17	0.42-0.51	17.65
	y	0.57-1.30	56.15	0.29-0.35	17.14
c-H-shaped	x	0.43-0.75	42.67	0.27-0.32	15.63
	y	0.68-1.59	57.23	0.44-0.56	14.29

**Table 2 The comparison of
Reflection properties of several kinds of different unit cell structure**

Unit cell structure	Polarized direction	f_{min}-f_{max} (THz)	Δf /f_{max} (%)	R_{min}-R_{max}	ΔR/R_{max} (%)
rectangular	x	1.31-2.60	49.62	0.02-0.06	66.7
	y	1.31-2.60	49.62	0.02-0.06	66.7
c-eSRRs	x	0.90-1.90	52.60	0.09-0.13	30.8
	y	0.62-1.30	52.31	0.17-0.22	22.73
c-H-shaped	x	0.38-0.72	47.22	0.19-0.24	20.83
	y	0.69-1.56	55.77	0.07-0.11	36.36

Table 1 and 2 show the transmission and reflection properties of the above several kinds of structure patterns, respectively. It can be found that the c-GSiO$_2$Si structures show good frequency modulation properties, the value of f_{mod} is about more than 50%. The reasons are shown in the following. For the resonant unit cell elements of the MMs structure, the resonant frequency can be expressed as ω_R=1/$(LC)^{1/2}$, L and C are the effective inductance and capacitance, respectively. The inductance includes the L_{sum}=L_g+L_k, L_g is the geometric inductance and related to the structure parameters of MMs, while the L_k is the kinetic inductance, $L_k \propto m_e/(n_e e^2)$, m_e is the electron mass, e is the electron charge and n_e is the carrier concentration. As the Fermi level of the graphene layer increase, the carrier concentration increases, resulting into the value of L_k decreases. Thus, the value of the L_{sum} decreases and the

resonance frequency shifts to the high frequency. Furthermore, in the THz regime the intra-band contribution dominants, the carrier concentration of the graphene layer increases significantly with the increase of the Fermi level. Consequently, the resonance frequency shifts to the high frequency significantly and can be can be modulated in a wide range with the increase of Fermi level. But the modulation depth of the transmission and reflection amplitude is not very much. The graphene MMs can show good modulation properties both along x and y directions, especially the rectangular-shaped structure show polarization insensitive properties due to the symmetrical structure. Another point should be noted is that the modulation depths for those several kinds of resonators are slightly different. From the fabrication viewpoint, it had better choose simple structure, such as the rectangular and H-shaped unit cell structure.

4. Conclusions

By depositing the planar arrays of graphene patterns on the SiO_2/Si/polymer substrate, the tunable propagation properties of the proposed c-GSiO$_2$Si structure have been given and discussed in the THz regime, including the influences of operation frequency, Fermi levels, and different kinds of graphene patterns. The study manifest that the tunable mechanisms of the c-GSiO$_2$Si structure mainly depend on the *LC* resonance, different from the original graphene MMs based on the dipolar resonance. By changing the Fermi level of the graphene layer, the transmission and reflection curves can be tuned in a wide range. As the Fermi level of graphene layer increases, the transmission resonance of the c-GSiO$_2$Si structure become stronger, and the resonant peaks shift to the higher frequency, resulting from the graphene permittivity increasing with Fermi level in the THz regime. The transmission (reflection) curve is broad (sharp), thus the c-GSiO$_2$Si structure can be used to fabricate transmission modulators (reflection filters). The results are very useful to design novel waveguides devices, such as modulators, filters and

switchers, and understand the mechanisms of the graphene plasmonic structures.

References

[1] B. S. Williams, *Nat. Photonics*, 2007, **1**, 517-525.

[2] J. T. Lü and J. C. Cao, *Appl. Phys. Lett.*, 2006, **89**, 211115.

[3] H. Li, J. C. Cao, J. T. Lü, and Y. J. Han, *Appl. Phys. Lett.*, 2008, **92**, 221105.

[4] J. C. Cao, *Phys. Rev. Lett.*, 2003, **91**, 237401.

[5] P. H. Siegel, *IEEE Trans. Microw. Theory.*, 2004, **52**, 2438-2447.

[6] B. Ferguson and X. C. Zhang, *Nat. Mater.*, 2002, **1**, 26-33.

[7] D. M. Mittleman, *Nat. Photonics*, 2013, **7**, 666-669.

[8] M. Choi, S. H. Lee, Y. Kim, S. B. Kang, J. Shin, M. H. Kwak, K. Y. Kang, Y. H. Lee, N. Park, and B. Min, *Nature*, 2011, **470**, 369-373.

[9] S. Linden, C. Enkrich, G. Dolling, M. W. Klein, J. Zhou, and T. Koschny, *J. Sel. Top. Quantum Electron.*, 2006, **12**, 1097-1105.

[10] S. Zhang, Y. S. Park, J. Li, X. Lu, W. L. Zhang, and X. Zhang, *Phys. Rev. Lett.*, 2009, **102**, 023901.

[11] X. Y. He, Q. J. Wang, and S. F. Yu, *IEEE J. Quantum. Electron.*, 2012, **48**, 1554-1559.

[12] Z. Li, Y. Ma, R. Huang, R. Singh, J. Gu, Z. Tian, J. Han, and W. L. Zhang, *Opt. Express*, 2011, **19**, 8912-8919.

[13] X. Y. He and H. X. Lu, *Nanotechnology*, 2014, **25**, 325201.

[14] F. Falcone, T. Lopetegi, M. A. G. Laso, J. D. Baena, J. Bonache, M. Beruete, R. Marqués, F. Martín, and M. Sorolla, *Phys. Rev. Lett.*, 2004, **93**, 197401.

[15] N. Landy, J. Hunt, and D. R. Smith, *Photonics and Nanostructures*, 2013, **11**, 453-467.

[16] B. Alavikia, T. S. Almoneef, and O. M. Ramahi, *Appl. Phys. Lett.*, 2014, **104**, 163903.

[17] P. Pitchappa, C. P. Ho, P. Kropelnicki, N. Singh, D. L. Kwong, and C. Lee, *Appl. Phys. Lett.*, 2014, **104**, 201114.

[18] J. M. Manceau, N. H. Shen, M. Kafesaki, C. M. Soukoulis, and S. Tzortzakis, *Appl. Phys. Lett.*, 2010, **96**, 021111.

[19] N. H. Shen, M. Massaouti, M. Gokkavas, J. M. Manceau, E. Ozbay, M. Kafesaki, T. Koschny, S. Tzortzakis, and C. M. Soukoulis, *Phys. Rev. Lett.*, 2011, **106**, 037403.

[20] H. T. Chen, J. F. O'Hara, A. K. Azad, A. J. Taylor, R. D. Averitt, D. B. Shrekenhamer, and W. J. Padilla, *Nat. Photonics*, 2008, **2**, 295-298.

[21] A. R. Wright and C. Zhang, *Phys. Rev. B*, 2010, **81**, 165413.

[22] X. Y. He and H. X. Lu, *Nanotechnlogy*, 2014, **25**, 325201.

[23] C. Wang, Y. Liu, L. Li, L. Lana and H. Tana, *RSC Adv.*, 2014, **4**, 9395.

[24] A. R. Wright, J. C. Cao, and C. Zhang, *Phys. Rev. Lett.*, 2009, **103**, 207401.

[25] X. G. Xu, S. Sultan, C. Zhang, and J. C. Cao, *Appl. Phys. Lett.*, 2010, **97**, 011907.

[26] F. H. L. Koppens, D. E. Chang, and F. J. G. de Abajo, *Nano Lett.*, 2011, **11**, 3370-3377.

[27] X. Y. He, J. Tao, and B. Meng, *Nanotechnology*, 2014, **24**, 345203.

[28] A. Vakil and N. Engheta, *Science*, 2011, **332**, 1291-1294.

[29] X. Y. He, *Opt. Express*, 2009, **17**, no. 17, 15359-15371.

[30] H. Yan, T. Low, W. Zhu, Y. Wu, M. Freitag, X. Li, F. Guinea, P. Avouris, and F. Xia, *Nat. Photonics*, 2013, **7**, 394-399.

[31] X. Y. He and R. Li, *IEEE J. Sel. Top. Quantum Electron.*, 2014, **20**, 4600106.

[32] L. Ju, B. Geng, J. Horng, C. Girit, M. Martin, Z. Hao, H. A. Bechtel, X. G. Liang, A. Zettl, Y. R. Shen, and F. Wang, *Nat. Nanotechnol.*, 2011, **6**, 630-634.

[33] X. Y. He, Z. Y. Zhao and W. Z. Shi, *Opt. Lett.*, published on line, www.opticsinfobase.org/ol/upcoming_pdf.cfm?id=225306.

[34] S. H. Mousavi, I. Kholmanov, K. B. Alici, D. Purtseladze, N. Arju, K. Tatar, D. Y. Fozdar, J. W. Suk, Y. Hao, A. B. Khanikaev, R. S. Ruo, and G. Shvets, *Nano Lett.*, 2013, **13**, 1111-1117.

[35] F. Valmorra, G. Scalari, C. Maissen, W. Fu, C. Schönenberger, J. W. Choi, H. G. Park, M. Beck, and J. Faist, *Nano Lett.*, 2013, **13**, 3193-3198.

[36] J. Ding, B. Arigong, H. Ren, M. Zhou, J. Shao, M. Lu, Y. Chai, Y. Lin, H. Zhang, *Sci. Rep.*, 2014, **4**, 6128.

[37] S. H. Lee, M. Choi, T. T. Kim, S. Lee, M. Liu, X. Yin, H. K. Choi, S. S. Lee, C. G. Choi, S. Y. Choi, X. Zhang, and B. Min, *Nat. Mater.*, 2012, **11**, 936-941.

[38] W. Gao, J. Shu, K. Reichel, D. V. Nickel, X. He, G. Shi, R. Vajtai, P. M. Ajayan, J. Kono, D. M. Mittleman, and Q. Xu, *Nano Lett.*, 2013, **14**, 1242-1248.

[39] Z. Y. Tan, T. Zhou, J. C. Cao, and H. C. Liu, *IEEE Photonic Technol. Lett.*, 2013, **25**, 1344-1346.

[40] V. P. Gusynin and S. G. Sharapov, *J. Phys. Condes. Matter.*, 2007, **19**, 026222.